January 2009

A Novel Model for (percolating) Nanonet Chemical Sensors for Microarray-based E-Nose Applications

J. Go

V. V. Sysoev

A. Kolmakov

N. Pimparkar

M. A. Alam

Go, J.; Sysoev, V. V.; Kolmakov, A.; Pimparkar, N.; and Alam, M. A., "A Novel Model for (percolating) Nanonet Chemical Sensors for Microarray-based E-Nose Applications" (2009). *Department of Electrical and Computer Engineering Faculty Publications.* Paper 57.
http://dx.doi.org/http://dx.doi.org/10.1109/IEDM.2009.5424266

A Novel Model for (percolating) Nanonet Chemical Sensors for Microarray-based E-Nose Applications

*J.Go , [1]V. V. Sysoev, [2]A. Kolmakov, N. Pimparkar, and M.A. Alam

*E-mail: go@purdue.edu, alam@purdue.edu Phone: (765) 413 8866 Fax: (765) 494 2706

School of Electrical and Computer Engineering, Purdue University, West Lafayette, IN 47907, USA
[1]Department of Physics, Saratov State Technical University, Saratov 410054, Russia; [2]Department of Physics, Southern Illinois University, Carbondale, Illinois 62901, USA

Abstract

Our numerical simulations for percolating multi-nanowire (NW) chemical sensors demonstrate the fundamental role of potential barriers at NW-to-NW junctions in dictating sensor response and how the sensor response changes with NW density. Based on this model, we explain the counterintuitive enhancement of detection limit at a high-density NW network sensor.

Introduction

Microarray-based solid-state gas sensors, usually made of metal oxides (e.g., SnO_2, ZnO, In_2O_3), have fundamentally different sensing mechanism than that of biosensors: First, for biosensors, no charge transfer occurs between substrate of the sensor and the biomolecule to be sensed, and the interaction is exclusively electrostatic [1], in contrast, chemical sensor relies on charge-transfer interaction [2]. Second, chemical sensors do not use the 'orthogonal' detection scheme typical of biosensing (derived from highly specific antibody-antigen, or DNA conjugation reactions [3]), but rather depend on distinct patterns of responses generated by a set of sensor elements in the array. These patterns can provide a fingerprint which allows identification of target analytes (Fig. 1) [4]. Given the complexity of the charge-transfer based detection scheme and corresponding pattern analysis, it is not surprising that the physical and predictive models of chemical-sensing are still in their early stages of development.

Recently it is often suggested that the enhanced surface-to-volume (S/V) ratio makes 1D nanowires (NWs) and nanotubes a sensitive detector of gas molecules for electronic nose (e-nose) and related applications [5,6]. However, this classical framework fails to explain why multi-NW sensors with lower S/V and higher density offer high sensitivity and very low detection limits [7-10]. In this paper, we use percolation theory to illustrate that it is the *resistive NW-to-NW junctions*, rather than the S/V ratio, that dictate the response of multi-NW chemical sensors. We establish a simple scaling law to relate the detection limit of multi-NW sensors to density of NWs (D_{NW}) that could allow the industry to quantitatively explore the viability and discriminating power of multi-NW arrays for microbiological, food safety and medical applications.

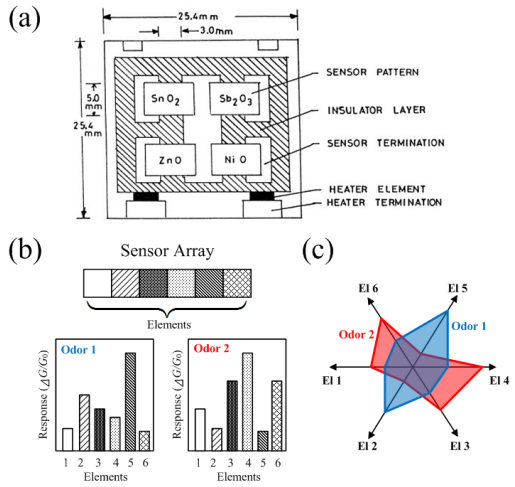

Fig. 1 (a) A typical microarray-based chemical sensors is composed of sensing elements with different materials. (b) Responses of an array of distinct sensing elements to different odors (left) and their corresponding fingerprints (right). Distinct patterns of fingerprints enable the discrimination of different odors, as shown in (c).

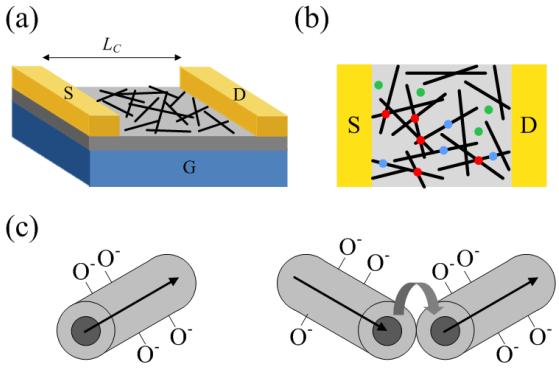

Fig. 2 (a) Schematic diagrams for multi-NW chemical sensors with a channel length of L_C. S, D and G are source, drain, and gate respectively. (b) Top view of Fig. 2a. The red, blue, and green dots represent O_x^-/OH^- species chemisorbed on the inter-wire junctions, NW surface, and oxide surface, respectively. The physisorbed atoms on the sensor surface (green dots) do not affect sensor conductance. (c) Electronic transport through the straight part of NW (left) and NW-NW junctions (right). The dark inner circles represent the 'squeezed' conducting channel due to depletion region at NW surface.

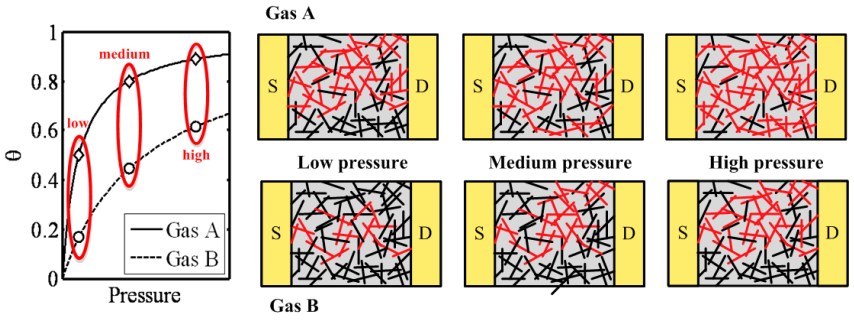

Fig. 3 Current paths across the network with varying partial pressure of target gas molecules with constant density of NWs. Red sticks indicate NWs which current flows through. The fraction θ of chemically-interacting oxygen vacancies follows Langmuir isotherm and is specific to the chemical properties of gas.

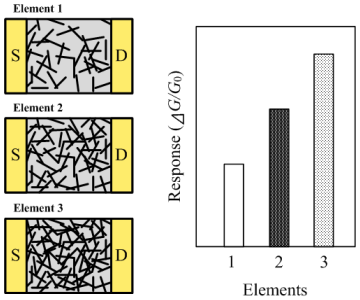

Fig. 4 Numerically calculated response of three distinct gas sensing elements with different NW densities (D_{NW}) at a given partial pressure of target gas. The channel length and stick length are fixed.

Device Modeling

Our numerical model generalizes the stick-percolation framework, originally developed to study the transport properties of nanonet Thin Film Transistors [11,12] (Fig. 2a). Like the previous work, this model populates a 2D grid by randomly-oriented sticks of uniform length (L_S). The initial current (I_{init}) is calculated by solving diffusion flux through the network of homogeneous NWs at low V_D (i.e., specifically the low bias drift-diffusion equation, $J = q\mu n\, d\varphi/ds$ is combined with current continuity equation, $dJ/ds = 0$), to find the equation for dimensionless potential φ_i along NW i as $d^2\varphi/ds^2 - C_{ij}(\varphi_i - \varphi_j) = 0$ where s is the length along the NW and $C_{ij} = G_M/G_S$ is the dimensionless charge-transfer coefficient between NWs i and j at their intersection, and G_M and G_S are mutual and self conductances of the wires, respectively. A 'poor' wire-to-wire is defined by small C_{ij} (« 1) and a perfect contact by $C_{ij} = 1$ [11].

To model NW gas sensor, one begins with a presumption of pre-existing oxidation of metal-oxide NW surfaces by O_x^-/OH^- species, which originate from atmospheric oxygen and/or water (Fig. 2b) [2]. We assume that the initial conductance (G_0) of metal-oxide NW sensor is determined by the interaction between NW surface and O_x^-/OH^- groups since depletion regions are formed by O_x^-/OH^- groups at NW surface. The depletion region populated at the *intersection* of two NWs creates potential barrier (ψ_B) that blocks electron transfer from one NW to another. Subsequent introduction of reducing analyte gas lowers ψ_B dramatically as the analyte gas molecules reduce the O_x^-/OH^- species to force it to return the trapped electron to the NW surface. The change of ψ_B is reflected in our model by enhanced C_{ij}. To compute the sensor conductance (G) after introducing target gas, we first use Langmuir isotherm $\theta = \alpha P/(1+\alpha P)$, where α is Langmuir coefficient and P is the partial pressure of target gas, to determine the fraction of junctions that would be reduced by target gas. These 'gas-reduced' junctions with low barriers (or high C_{ij}) are randomly populated across the network so that $G \sim f(P)$, as shown in Fig. 3. This approach allows us to compute sensor $\Delta G/G_0$ as a function of partial analyte pressure as well as network density (Fig. 4). An ensemble of responses produced by a sensor array (each of which is characterized by a gradient in the density of sticks) eventually allows us to obtain the fingerprints of given gas molecules.

In our simulation (i) first we randomly populate sticks on 2-D plane to generate a random network (ii) and then

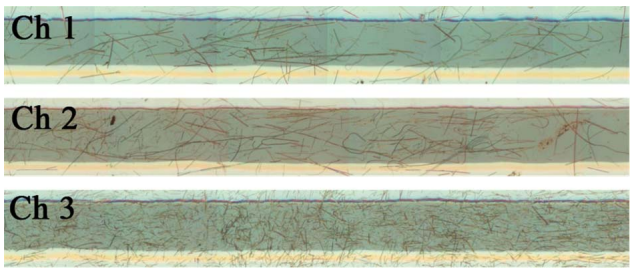

Fig. 5 High-resolution optical images of three different sensing elements: Ch1, Ch2, and Ch3 [13]. The density of NW (D_{NW}) and average wire length (L_S) is 0.0022 μm^{-2} and 46.15 μm for Ch1, 0.0031 μm^{-2} and 41 μm for Ch2, 0.0204 μm^{-2} and 13.75 μm for Ch3. The channel length is 70 μm for all three channels. Their corresponding normalized densities, which can be defined as $D_{NW} \times L_S^2$, are 4.686, 5.211, and 3.857: the order of magnitude is the same as the normalized density shown in Fig. 8.

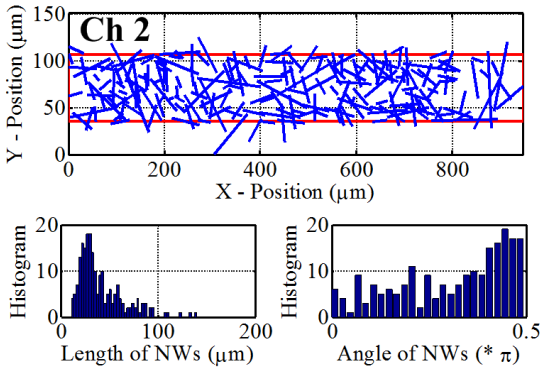

Fig. 6 Extraction of device geometry parameters from the image of Ch2 (Fig. 5). We take the average length of NW for simulation. The average angle of NWs, estimated as 0.246 × π, shows that the NWs are randomly oriented.

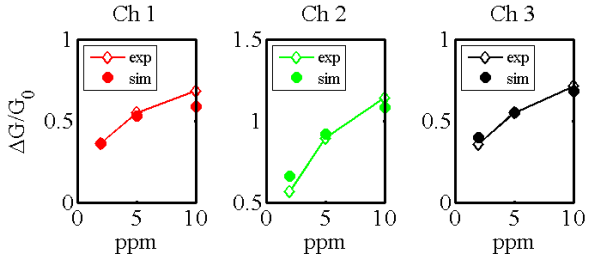

Fig. 7 Comparison between experiment [13] and simulated response of chemical sensors for 2-propanol gas in the constant temperature condition. Ch1, Ch2, and Ch3 represent three different sensor segments with distinct NW densities and average NW lengths. The fitting parameters we used are: $C_{ij}^{0} = 5 \times 10^{-4}$, $C_{ij}^{oc} = 1$, $\alpha = 0.5$ ppm^{-1}. The series resistance (R_S) we assumed for Ch1, Ch2, and Ch3 are 0.9 MΩ-μm, 1.5 MΩ-μm, and 692 MΩ-μm respectively.

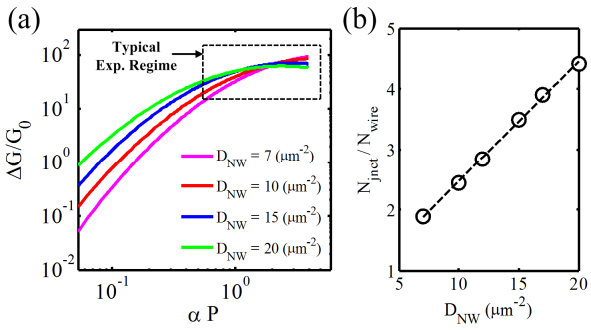

Fig. 8 (a) The ensemble-averaged sensor response as a function of αP with different NW densities. The channel length (L_C) and NW length (L_S) are fixed as 2 μm and 1 μm, respectively. The values of C_{ij}^{0} and C_{ij}^{oc} are $C_{ij}^{0} = 5 \times 10^{-4}$, $C_{ij}^{oc} = 1$. (b) The ratio of the number of NW-NW junctions (N_{jnct}) to that of wires populated between two electrodes (N_{wire}).

randomly select junctions in the network according to a given value of fraction θ, (iii) alter the C_{ij} values of chosen junctions to reflect chemical reactions of gas, and finally (iv) solve transport equation for the network. We consider the effect of gas molecules at the junctions and do not take into account the variation of depletion layer width in a NW body, because we find that the surface effect is negligible compared to the 'junction' effect.

Model Calibration

To calibrate the model parameters, we first use a high-resolution optical images (Figs. 5, 6) from Ref. [13] to determine D_{NW} and average NW length (L_S) for sensors. Next, we simulate an ensemble of 1000 samples of NW network with D_{NW} and L_S we obtained previously to calculate ensemble-averaged conductance (G_0) at oxygen-rich atmosphere before the introduction of target gas. We then estimated several parameters to fit the experimental response curve [13]: the Langmuir coefficients of target gas molecules, the magnitude of C_{ij} before (C_{ij}^{0}) and after (C_{ij}^{oc}) molecular adsorption, and series resistances. In the estimation we assume that (a) initially *every* NW-to-NW junction prior the gas chemisorption has high resistance ($C_{ij}^{0} \ll 1$) due to O_x^-/OH^- species and that (b) a fraction of the NW-NW contact becomes perfect ($C_{ij}^{oc} = 1$) due to chemical reactions by introducing target gas. The theoretical predictions from the calibrated model compares very well with experiments (Fig. 7). This calibrated model, with no further changes in C_{ij}, are now used to study the effect of target gas partial pressure and D_{NW}.

Results and Discussions

After validating our model by comparing to experimental results we now compute the sensor response as a function of network density D_{NW} with respect to the product of Langmuir constant and partial gas pressure, αP, as a scaling variable. Remarkably, the simulation results show larger magnitude of sensor response with denser network of nanowires (Fig. 8a), in general agreement with the reported experimental results [14]. Combined with our numerical studies regarding the number of junctions as a function of NW density (Fig. 8b), this provides the first quantitative explanation for this effect and validates the hypothesis that it is the 'junction' effects, rather than the 'S/V' effect which dictates the response of

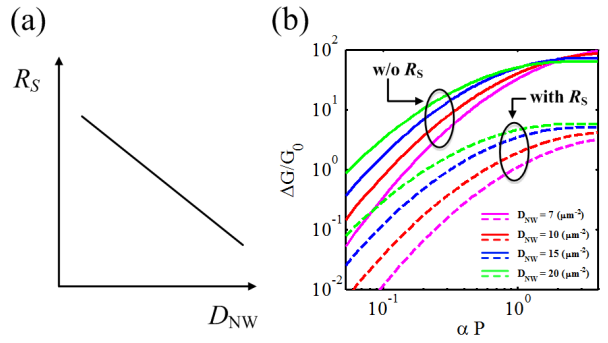

Fig. 9 (a) Contact series resistance (R_S) of multi-NW sensor with respect to D_{NW}. High R_S for Ch3 (Fig. 7) can be explained by the negative dependence of R_S on D_{NW}. (b) Degradation of sensor responses from Fig. 8a (solid lines) due to the series resistance (dotted lines) between electrodes and its contacting NWs. Sparser network (less D_{NW}) suffers higher degradation due to its large contact series resistance.

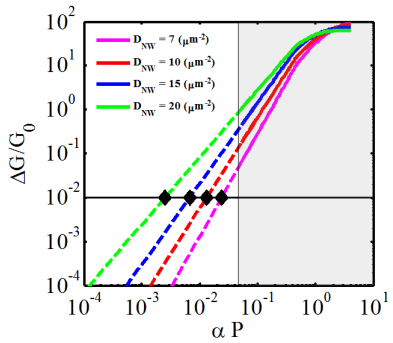

Fig. 10 The power-law relationship between sensor response and gas pressure at low-pressure regime. The dotted lines represent extrapolation of numerically-computed sensor responses (solid lines in shaded region, from Fig. 8a) at $\alpha P < 1$. We assume that the minimum magnitude of detectable response for a gas sensor is 10^{-2} (horizontal line) and black diamond symbols represent detection limits for different NW densities.

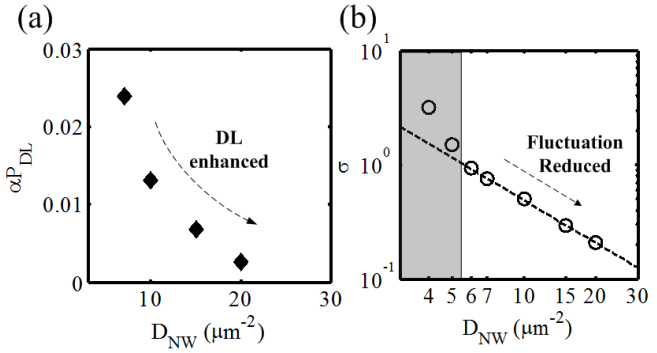

Fig. 11 (a) Predicted detection limit of chemical sensors, denoted as αP_{DL}, with respect to the NW density from Fig. 10. The detection limit is enhanced about one order of magnitude by raising NW density only by a factor of three. (b) Normalized standard deviation (σ) of channel current with network density from 1000 ensemble of multi-NW sensors. The shaded part represents the regime under percolation threshold. Detection limit and element-to-element fluctuation both improve at higher NW density.

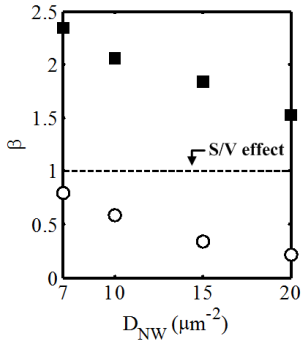

Fig. 12 Relationship between power exponent (β) vs. D_{NW} for αP « 1 (black squares) and αP ~ 1 (white circles) in Fig. 10. The power exponent has a negative dependence on D_{NW} where the power exponent due to S/V effect is constant regardless of D_{NW}.

nanowire chemical sensors. [7,13,14].

One of the interesting consequences of the 'stick-density' dependent nanonet sensor response is that the gradient of nanowire density across individual sensing segments provides sufficient discrimination power of gas sensor microarrays with no additional gradient parameter such as temperature [13], typical of more traditional chemical sensor setup. In terms of sensor operations, density control is cost-effective compared to temperature control and it simplifies the sensor design considerably.

The most interesting implications from our numerical studies are (i) a simple scaling law of sensor response, $\Delta G / G_0 \sim (\alpha P)^{\beta(D_{NW})}$, at low pressure regime (αP « 1, Fig. 10) such that power exponent $\beta(D_{NW})$ reduces with higher D_{NW} and (ii) the enhancement of detection limit (αP_{DL}) at a high-density network (Fig. 11a). Although $\beta(D_{NW})$ itself is dependent on the chemical properties of target gas molecules, sensor materials, and geometry of sensor as well, the trend of power exponent predicts that the detection limit can be improved simply by raising the network density *without any aid of surface functionalization*. In addition, the magnitude of power exponents ($\beta(D_{NW}) > 1$, Fig. 12) in the limit of low partial pressure validate our assumption that the sensor response due to interwire junctions changes more dramatically than any depletion effects associate with bulk, NW since the latter is only *linearly* proportional ($\beta = 1$, Fig. 12) to the low partial pressure of target gas [15]. The physical origin of dramatic changes at low pressure regime (αP « 1) is that *every* reducing target molecule interacting with junctions contributes new conduction pathways through the network. At high pressure regime (αP ~ 1), in contrast, the number of target molecules are sufficient to populate all the major pathways and additional increase of partial pressure only contribute to creation of subbranches for pre-existing paths, with an overall reduction in the magnitude of power exponents ($\beta(D_{NW}) < 1$, Fig. 12).

Conclusion

We have conclusively demonstrated for the first time the fundamental role of potential barriers at wire-to-wire junctions in dictating gas sensor response and how the conductance of sensors changes with NW network density. Based on this model, we have also provided the first intuitive explanation of the enhancement of detection limit at a high-density network sensor. The dependence of sensor response on the network density explains a discrimination power of gas sensor microarrays with gradient density of NWs across the sensor and its feasibility for various applications.

References

[1] Nair *et al*., *Nano Lett*., p. 1281, 2008. [2] Barsan *et al*., *J. Electroceram*., p. 143, 2001. [3] Zheng *et al*., *Nat. Biotechnol*., p. 1294-1301, 2005. [4] Albert *et al*., *Chem. Rev*., p. 2595, 2000. [5] Chen *et al*., *IEEE Trans. Nanotechnol*., p. 668, 2008. [6] Comini *et al*., *Prog. Mater Sci*., p. 1, 2009. [7] *Zhang* et al., *Nano Lett*., p. 1919, 2004. [8] Comini *et al*., *Appl. Phys. Lett*., p. 1869, 2002. [9] Kim *et al*., *Nano Lett*., p. 2009, 2006. [10] Sysoev *et al*., *Sens. and Actuators B*., p. 699, 2009 [11] Pimparkar *et al*., *65th Device Research Conference*, p. 17, 2007. [12] Kumar *et al*., *Phys. Rev. Lett*., p. 066802, 2005. [13] Sysoev *et al*., *Nano Lett*., p. 3182, 2007. [14] Hwang *et al*., *Sens. Actuators B*, p. 224, 2009. [15] Fan *et al*., *Appl. Phys. Lett*., p. 123510, 2005.